Journal of Materials Chemistry C

Accepted Manuscript

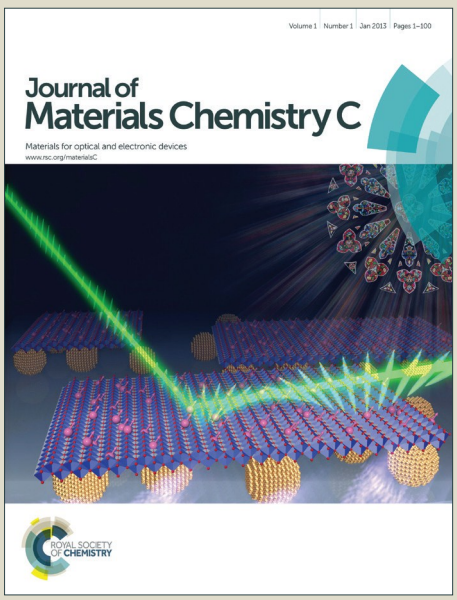

ROYAL SOCIETY OF CHEMISTRY

www.rsc.org/materialsC

Synthesis of Graphene Oxide Dots for Excitation-Wavelength Independent Photoluminescence at High Quantum Yields

Chiao-Yi Teng,[a] Te-Fu Yeh,[a] Kuang-I Lin,[b] Shean-Jen Chen,[b,c] Masahiro Yoshimura,*[, d] and Hsisheng Teng*[,a,b]

[a]Department of Chemical Engineering and Research Center for Energy Technology and Strategy, National Cheng Kung University, Tainan 70101, Taiwan

[b]Center for Micro/Nano Science and Technology, National Cheng Kung University, Tainan 70101, Taiwan

[c]Department of Engineering Science, National Cheng Kung University, Tainan 70101, Taiwan

[d]Promotion Center of Global Materials Research and Department of Materials Science and Engineering, National Cheng Kung University, Tainan 70101, Taiwan

*To whom correspondenec should be addressed. E-mail: hteng@mail.ncku.edu.tw,

Tel: 886-6-2385371, Fax:886-6-2344496

Abstract

This study reports on the synthesis of graphene oxide dots (GODs, 2.5±0.5 nm) exhibiting excitation-wavelength independent photoluminescence (PL) at 530 nm. The GODs, which are of high uniformity and crystallinity, are produced by mildly oxidizing thermally-reduced GO sheets under sonication. The GOD aqueous suspension yields a maximal PL quantum yield (*QY*) of 16 % under excitation at 470 nm. This PL can be ascribed to the irradiative excitation of electrons from the non-bonding oxygen (n) states to the graphene anti-bonding π orbital with subsequent relaxation of the electrons to the n ground states. Nitrogen-doping reduces vacancy defects and donates electrons to compensate for the unbalanced charge in p-type GODs, thereby increasing the PL *QY* to 22 % for the nitrogen-doped GODs (NGODs). Treating the unadorned GODs and NGODs with submerged liquid plasma in tetrahydrofuran suppresses charge leakage from the carbonyl groups on the graphene periphery and increases the *QY*s to 42 % and 50 %, respectively. The GODs could be used as a phosphor for the generation of white light by combining green emissions (530 nm) with violet light used for excitation. The present study demonstrates facile synthesis of high-quality green-emitting GODs and an effective method for the repair of vacancy defects and the stabilization of oxygen functionalities to enhance PL emission from GODs.

Keywords: Graphene oxide dots; Photoluminescence; Green-light emission; Phosphor

1. Introduction

Fluorescent carbon materials have attracted considerable attention due to their low toxicity, excellent biocompatibility, low cost, high resistance to photobleaching, and an abundance of raw materials in nature.[1-11] Among the various carbon structures, graphene-derived materials offer particular advantages resulting from their unique 2D carbon grid skeleton, which allows extensive modification with surface functionalities.[12] Making a π-network in graphene of infinite to finite size creates band gaps and imparts fluorescence.[6,13-17] Size reduction and chemical modification are the most common strategies for the creation of a band gap in graphene-based materials. Integrating these two approaches results in the formation of graphene oxide dots (GODs), a material ideally suited to applications requiring photoluminescence (PL).[3-5,7,18] Improving the PL performance of GODs requires modulating their electronic structure through the regulation of oxygen functionalities or heteroatom doping in order to facilitate the recombination of photoexcited charges.

Most GODs emit blue light under UV excitation,[19-35] which seriously limits their scope of applicability. The ability to produce GODs capable of emitting other colors would be highly desirable, particularly for the development of devices requiring white light emission.[36,37] Blue PL in GODs was traced back to free zigzag sites with a carbine-like triplet ground states designated as $\sigma^1\pi^1$.[7] Another study reported the emission of blue light under UV illumination from reduced GO containing few free zigzag sites.[38] Despite the wide range of PL mechanisms that have been proposed, most researchers agree that the irradiative recombination of electron-hole pairs confined in sp^2 clusters yield blue light emissions.[6] GODs comprise an sp^2 domain that renders high carrier transport mobility as well as disordered sp^3

hybridized carbon atoms, which bind to oxygen-containing functional groups at edge sites. Green PL from GODs may originate in these disordered edge states.[39-47] A study proposed a mechanism to explain PL in fluorescent GODs, in which the state of functional groups was responsible for the green fluorescence whereas intrinsic sp^2-cluster states emitting blue light could be inherited from its precursor GO.[48] Correlating the charge-transfer mechanisms involved in the blue and green PL of GODs could provide valuable insight into the electronic framework underlying the processes of optical absorption and emission in GODs.

In addition to the functionalization of graphene using oxygen atoms, the insertion of heteroatoms such as nitrogen and boron provides high-stability doping through the formation of covalent bonds with sp^2 carbon in the aromatic network.[49-51] Nitrogen-doped graphene has been widely studied for its enhanced electrochemical properties.[51] Nitrogen insertion in graphene forms sp^2-hybridized quaternary and/or pyridinic or sp^3-hybridized pyrrolic bonding configurations through the donation of one or two p-orbital electrons to the π system,[51] which conveys n-type conductivity to the graphene.[49] The change in the type of conductivity in GO resulting from nitrogen doping is a major factor in the performance of GO with regard to photocatalysis and photoluminescence.[52] Surface functionalization or modification using macromolecules has also been employed to minimize the occurrence of surface defects in order to promote the PL intensity of GODs.[9,20,53-55] The solvent molecules used to disperse GODs also influence surface passivation.[56,57]

In this study, we synthesized GODs using mild oxidation along with sonication to regulate the physical and chemical uniformity of the dots. The GODs provide green light emissions under UV and visible irradiation irrespective of the excitation wavelengths. Nitrogen doping eliminates vacancy defects and creates n-type domains

in the GODs, which enhance the PL emission of the resulting nitrogen-doped GODs (NGODs). We then treated the NGODs with submerged liquid plasma (SLP) in tetrahydrofuran (THF) to passivate the oxygen functionalities.[58-61] This resulted in an increase in PL quantum yield (*QY*) to 50 %. Our results demonstrate the effectiveness of SLP treatment in the surface passivation of phosphor powders. The correlation between the electronic structure and the optical properties of GODs illustrates the charge-transfer mechanism underlying the PL in GODs. Our findings demonstrate the applicability of GODs as phosphors for white light-emitting devices.

2. Experimental

2.1. Preparation of Materials

GO was prepared using a modification of Hummers' method with natural graphite powder (Bay carbon, SP-1, USA). Graphite powder (5 g) and $NaNO_3$ (2.5 g; Merck, Germany) were added to a solution of concentrated H_2SO_4 (18 M, 115 mL; Wako, Japan) in an ice bath. $KMnO_4$ (15 g, J.T. Baker, USA) was gradually added under stirring with the temperature of the mixture held below 20 °C. The mixture was then stirred at 35 °C for 4 h to allow oxidation. Deionized water (230 mL) was slowly added to the mixture and stirred at 98 °C for 15 min before being further diluted to 700 mL and stirred for 30 min. The reaction was halted by the addition of H_2O_2 (12 mL, 35 wt%; Shimakyu, Japan) under stirring at room temperature. Multiple washings were conducted using deionized water (3 × 500 mL), and the precipitate of the final slurry was dried at 40 °C for 24 h to obtain the GO specimens.

Nitrogen-doped graphene (NG) was synthesized by treating as-prepared GO in a flow of NH_3 gas at 500 °C for 3 h. The NG sample was oxidized in concentrated HNO_3 at room temperature for 12 h. The solution was subsequently treated ultrasonically for 10 h. The mixture was heated in an oven to 140 °C and where it was held for 12 h to form NGODs. Unadorned GODs (uGODs) and boron-doped GODs (BGODs) were also prepared using roughly the same method except for the substitution of NH_3 treatment with Ar treatment at 500 °C to produce uGODs and with boron oxide treatment in Ar at 800 °C to produce BGODs. These GOD specimens were dispersed in deionized water to form suspensions of NGODs, uGODs, and BGODs. The suspensions used for optical analysis had a GOD concentration of 5 μg/mL

Submerged liquid plasma (SLP) treatment of the GODs was conducted for suspensions of the GODs in THF. In this plasma treatment, a tungsten needle was used as a point high-voltage electrode and Pt foil was used as a planar ground electrode. These experiments were conducted at ambient temperature by immersing both electrodes into the THF solutions suspending the GODs. A discharge voltage of 2.7 kV was applied across the electrodes using a pulse generator (Avtech AV-1022-C, Taiwan) connected to a high-voltage amplifier (Trek 609E-6, USA). Plasma treatment was applied for 10 min to obtain SLP-NGODs and SLP-uGODs, which were then dispersed in water to form aqueous suspensions for further analysis.

2.2. Methods of Analysis and Measurements

X-ray photoelectron spectroscopy (XPS; Kratos AXIS Ultra DLD, UK) with Al K_α radiation was used to quantitatively analyze the chemical composition of the GO-based samples. Raman spectra were recorded using a DXR Raman microscope

(Thermo Fisher Scientific Inc., USA) at room temperature under a laser with an excitation wavelength of 532 nm. A high-resolution transmission electron microscope (Jeol 2100F, Japan), equipped with a field-emission gun operating at 200 keV was used to investigate the microstructure of the samples. The topography of the samples was analyzed using atomic force microscopy (AFM; Digital Instrument Nanoscope IIIa, USA) in tapping mode. Samples used in AFM measurements were deposited on mica substrates. The optical absorption spectra of suspensions were obtained by placing the solutions in a 1-cm quartz cuvette and using a Hitachi U-4100 (Japan) spectrophotometer for analysis. The PL and photoluminescence excitation (PLE) spectra of the suspensions were measured at ambient temperature using a fluorescence spectrophotometer (Hitachi F-700, Japan) equipped with Xe-lamp excitation and 900/mm grating. The slit widths for excitation and emission were 20 and 10 nm, respectively.

The conductivity type of the samples was analyzed using an electrochemical impedance spectroscope (Zahner IM6e, Germany) in conjunction with Thales software. The samples were deposited on a glassy carbon electrode using drop-casting and electrochemical analysis was performed in a 0.5-M H_2SO_4 solution using a Pt-foil counter with reference Ag/AgCl electrode. Measurement involved the application of a sinusoidal potential perturbation with a small amplitude (10 mV), superimposed on a fixed DC potential, which varied within a potential window from −1 to 1 V (vs. Ag/AgCl).

3. Results and Discussion

3.1. Physical and Chemical Characteristics of GODs

Fig. 1a presents a transmission electron microscopy (TEM) image of as-prepared NGOD particles with particle size of 2.5±0.5 nm and narrow size distribution, as shown in Fig. 1b. The high resolution TEM image in Fig. 1c shows the round shape and crystalline lattice fringes of an NGOD particle. The interlayer spacing of 0.214 nm corresponds to the d-spacing of the graphene $\{1\bar{1}00\}$ planes. Selective area electron diffraction patterns of the NGOD (Fig. 1d), projected perpendicularly to the graphene basal plane, exhibit clear diffraction spots identical to those of graphite along the [0001] direction, indicating the high crystallinity of the NGODs. Fig. 2a presents an atomic force microscopy (AFM) image of NGODs. The height of most of the topographic features was between 0.5 and 2 nm with a mean height of 1.2 nm (Fig. 2b), suggesting that most of NGODs are single- or bi-layered.[3,4] The size, morphology, and crystalline structure of unadorned GODs (uGODs) presented little difference from those of NGODs.

This study used X-ray photoelectron spectroscopy (XPS) to determine the chemical composition of uGODs and NGODs. The full-range XPS spectrum of NGODs (Fig. 3a) presents binding energy peaks of C 1s at 284 eV, N 1s at 400 eV, and O1s peak at 532 eV. Mn impurities that originate from the preparation stage might be present,[62] but the XPS analysis did not find any Mn 2p peaks (642-654 eV).[63] The XPS analysis results of uGODs are presented in Fig. S1 of the ESI†. The O/C atomic ratio of NGODs determined by the full-range XPS spectrum was approximately 0.5, which is similar to that of uGODs (Table 1). The N 1s peak visible in Fig. 3a confirms that N atoms were successfully incorporated into the graphene oxide sheets via NH_3 annealing; however, the concentration of nitrogen was low. The

N/C atomic ratio of NGODs (ca. 0.04) was close to those of the nitrogen-doped carbon nanotubes[64] and graphene[65] prepared under similar NH_3 treatment conditions.

The de-convoluted C 1s XPS spectrum of NGODs (Fig. 3b) indicates the presence of oxygen-containing groups, C–O (285.7 eV), C=O (287.1 eV), and O–C=O (289.3 eV). The C–O bonds can be attributed to the epoxy and tertiary alcohol functional groups on the basal plane, as well as phenol and ether in the periphery. The C=O and O–C=O bonds indicate the presence of ketone, aldehyde, carboxyl, and ester groups in the graphene periphery. The high C=O concentration (Table 1) reflects the fact that most of the oxygen functionalities are located on the graphene sheet edge. As for the nitrogen functionalities, the de-convoluted N 1s spectrum of the NGODs (Fig. 3c) reveals the presence of pyridine-like (397.5 eV), pyrrolic-like (398.8 eV), and quaternary (399.4 eV) nitrogen atoms. The high percentages of pyridine- and pyrrolic-like functionalities indicate that most of the nitrogen atoms were located at the edge of the graphene sheets; however, the quaternary nitrogen atoms doped into the graphene lattice account for approximately one third of the nitrogen content.

SLP treatment in THF produced substantial variations in the composition of the oxygen-functionalities associated with the NGODs, but only slightly modified the oxygen and nitrogen contents (see the O/C and N/C ratios of Table 1). Fig. 4 presents an XPS spectrum showing the C 1s of SLP-NGODs. Table 1 lists the composition of the oxygen-containing groups obtained from the de-convolution of the C 1s spectrum. SLP treatment in THF substantially reduced the C=O content of NGODs from 22 % to 8.4 %. Table 1 reveals that the C–O and O–C=O groups increased at the expense of a loss of C=O. These results indicate that the ketone or aldehyde groups interacted with the THF molecular ring to form phenol, ether, and carboxyl groups on NGODs.

SLP treatment initiated this interaction, likely due to dissociation of C–H bonds on THF molecules resulting in the formation of active radicals.[66,67]

Raman spectroscopy was used to identify the graphitic structures of uGODs, NGODs, and SLP-NGODs. Fig. 5 shows that all of the samples exhibited the sp^3-associated disorder band (D) at 1380 cm^{-1}, in-plane sp^2 vibration crystalline band (G) at 1620 cm^{-1}, and vacancy-like bond-deformation defect band (D') at 1653 cm^{-1}.[68] The appearance of the double-resonant 2D band (2728 cm^{-1}) indicates that the uGODs and NGODs comprise orderly stacked graphene sheets.[69,70] The shape of these 2D bands reveals that these samples consist of graphene of approximately three layers, according to the double-resonant Raman model.[70] The G/D intensity ratios of these samples are similar (0.55). Nitrogen doping reduced the intensity of the D' band, suggesting that the vacancy defects of the uGODs had been repaired with N atoms following annealing in NH_3.[69] SLP treatment in THF further lowered D' band intensity, indicating that the THF molecules interacted with the NGODs resulting in the repair of a number of vacancy sites at the graphene-sheet periphery.

3.2. Influence of Doping and SLP Treatment on Optical Properties of GODs

Fig. 6 presents the absorption spectra of the NGOD and SLP-NGOD suspensions. All of the samples used in the present study, regardless of whether they were doped with nitrogen or boron, exhibited absorption patterns similar to those shown in Fig. 6. The NGOD solution absorbed UV and visible light and showed an absorption onset at ca. 800 nm (Fig. 6a). The spectrum revealed strong absorption resulting from the $\pi \rightarrow \pi^*$ transition in the sp^2 domains of NGODs at ca. 300 nm (3.8 eV).[7] A vague absorption shoulder at ca. 400–500 nm corresponds to electron transition from the n-states (i.e., the non-bonding oxygen states associated with the

C=O or C–O groups) to the π* states.[6,14,71,72] The low molar absorptivity associated with the n → π* transition caused the weak absorption shown in Fig. 6a.[73] The SLP-NGOD solution exhibited a slight red-shift of the π → π* absorption peak to 310 nm (Fig. 6b), which can be attributed to the electron withdrawing effect caused by the SLP-introduced carboxyl groups.[73]

Fig. 7a presents the PL emission peaks of the NGOD aqueous suspension excited by irradiation at various wavelengths. The PL emission results of the uGOD suspension are presented in Fig. S2a of the ESI†. Both samples exhibited strong visible-light PL emission at 530 nm, irrespective of the excitation wavelength. The short wavelength region of the PL spectra simply exhibits the interference from the excitation light and is removed from the spectra (see Fig. S2b for the full-range PL spectra of the NGOD suspension). Strong PL emissions occurred under excitation at 470 nm (2.6 eV), which corresponds to the energy gap between the π* and n states. The PL emission of NGODs was stronger than that of uGODs, likely due to removal of vacancy states by nitrogen doping. In addition, replacing carbon with nitrogen or introducing amine groups at the periphery of GO sheets would result in the donation of electrons to the carbon grid.[74] This electron donation may passivate the defects caused by electron deficiency by having the oxygen-containing groups withdraw electrons from the carbon grid of the GO.

We analyzed the results of electrochemical impedance spectroscopy using the Mott-Schottky equation (see the ESI†) to identify the type of conductivity in NGODs and uGODs. Fig. 8a presents the capacitance values of the space charge region in NGODs obtained at various applied potentials. According to the Mott-Schottky equation, the relationship of $1/C^2$ versus applied potential should be linear. Fig. 8a presents straight lines with negative and positive slopes located in different potential

regimes. The negative and positive slopes correspond to p- and n-type conductivities, respectively. The uGODs specimens exhibit only p-type conductivity (Fig. 8b). The co-existence of p- and n-type conductivities in NGODs indicate that nitrogen-doping resulted in the donation of electrons to produce n-type conductivity and compensated for the unbalanced charge in the electron-deficient sp^2 domain, thereby promoting irradiative recombination. As illustrated in Raman analysis, the elimination of the D' band via nitrogen doping (Fig. 6) confirms that nitrogen doping had repaired the defect states of uGODs through the donation of electrons. Previous studies have reported that electron-hole recombination in GO is generally the result of electronic transition among sp^2 clusters and the boundary of oxidized regions.[6,40,75] Thus, the nitrogen-repaired sp^2 clusters of NGODs may be responsible for the enhancement of PL emissions (compare Fig. 7a and S2a). The p-n junction in NGODs may also result in the non-irradiative Auger recombination, but this influence would be minor because the Auger recombination is a three-carrier process and does not easily occur.

Boron atoms have a smaller valence number than do carbon atoms; therefore, doping with boron atoms could potentially aggravate the charge unbalance in the electron-deficient sp^2 domains of GODs. We measured the PL emission of boron-doped GODs (BGODs) and compared the results with those of uGODs and NGODs. As shown in Fig. S3a of the ESI†, the intensity of PL emission is ranked as follows: BGODs < uGODs < NGODs. The green emission is the only one from all samples; doping did not result in other exciton recombination pathway (see Fig. S3b for the full-range PL spectra of the BGOD suspension and Fig. S2b for those of the NGOD). This justifies the use of electron donation to minimize charge unbalance in order to enhance the PL emission of GO-based materials; on the contrary, doping with low-

valence atoms could exacerbate the charge deficiency and thereby suppress PL emissions.

The SLP treatment in THF substantially enhanced PL emissions from the GODs. Fig. 7b presents a comparison of the PL spectra of uGODs and NGODs, either without or with the SLP treatment, under 470-nm excitation; the insets present photographs of the excited suspensions that exhibit green PL emissions. The SLP-treated GODs exhibit stronger emissions, compared to those of untreated GODs. Electrochemical impedance spectroscopic characterization revealed that the SLP treatment had little influence on the conductivity properties of the GODs, likely due to the little change in the oxygen and nitrogen contents. Thus, we can surmise that interaction with THF molecules passivated the surface of the NGODs, thereby enhancing irradiative charge recombination. As shown in Table 1, SLP-NGODs present a lower C=O content than do NGODs, indicating that C=O groups may have acted as leakage sites for charge transfer into the liquid phase, resulting in the suppression of PL emissions. Previous studies on electrochemical capacitors have identified carbonyl and quinone-type C=O groups as electron-drawing sites responsible for Faradaic redox charge transfer and storage,[76,77] according to the following equation:

$$>C_xO + e^- + H^+ \rightarrow >C_xOH \qquad (1)$$

where $>C_xO$ represents a quinone-type site and $>C_xOH$ a hydroquinone-type complex. The hydroxyl and phenolic C–O and carboxyl O–C=O groups had only acidic/basic activity.[76] Table 1 reveals that the C=O loss in the SLP treatment was accompanied by increases in C–O and O–C=O. The suppression of charge transfer via a reduction in C=O content is likely responsible for the high PL emissions of SLP-NGODs. Fig. 7b

also reveals that the advantageous nitrogen-doping effect was maintained after the SLP treatment.

The SLP-treatment results indicate that THF molecules interact with active ketones or aldehydes on the NGODs to form stable ethers, alcohols, or esters through reactions R1–R4, as shown in Fig. 9. The aforementioned oxygen functionalities containing non-bonding oxygen atoms are capable of serving as n states for irradiative charge recombination; however, the aldehydes and ketones that comprise carbonyl or quinine functionalities are active in charge transfer at the carbon-liquid interface.[72] The transformation of aldehydes and ketones to the other stable functionalities through reactions R1–R4 with THF molecules may have suppressed charge transfer and increased the probability of irradiative recombination. SLP treatment provided the energy necessary to expedite R1 for the conversion of aldehyde and ketone.

The PL quantum yields of the samples were calculated using the following equation,[78]

$$QY_x = \left(\frac{I_x}{I_{st}}\right)\left(\frac{\eta_x^2}{\eta_{st}^2}\right)\left(\frac{A_{st}}{A_x}\right)QY_{st} \qquad (2)$$

where I is the measured integrated emission intensity, η is the reflective index of the solvent, and A is the optical absorption density. Subscript "st" refers to a standard with known quantum yield ($QY_{st} = 0.79$ here by using a fluorescein-ethanol solution[79]) and "x" refers to a sample. In order to minimize re-absorption, absorbance in the 10×10 mm fluorescence cuvette was kept below 0.1 at an excitation wavelength 470 nm. The PL QY values under 470-nm excitation were as follows: 16 % for uGODs, 22 % for NGODs, 42 % for SLP-uGODs, and 50 % for SLP-NGODs. The values of the parameters for the QY calculation are provided in the ESI†. Our PL results

demonstrate the importance of nitrogen-doping in the repair of vacancy defects and SLP-treatment in converting electron-drawing C=O groups.

3.3. Charge-Transfer Mechanism Underlying the PL in GODs

Fig. 10 presents a schematic diagram illustrating the energy levels associated with PL emissions from GO. The PL of GO may originate from four types of electronic transition between anti-bonding and bonding molecular orbitals;[80,81] i.e., (i) the $\sigma^*\rightarrow\sigma$ electronic transition for alkane-like sp^3 domains, (ii) the $\sigma^*\rightarrow n$ transition that occurs in the sp^3 domains associated with hydroxyls, amines and ethers, (iii) the $\pi^*\rightarrow\pi$ transition that usually takes place in aromatic sp^2, and (iv) the $\pi^*\rightarrow n$ transition that is typically observed in sp^2 domains adjacent to ether, ketone, carboxyl, and ester groups. The NGOD absorption spectra in Fig. 6 depicts the marked absorption characteristics associated with the $\pi^*\rightarrow\pi$ and $\pi^*\rightarrow n$ transitions. The PL spectrum in Fig. 7a indicates that excitation at 470-nm for the $n\rightarrow\pi^*$ transition followed by relaxation and an irradiative 530-nm recombination transition was responsible for the strongest PL emissions. The photoluminescence excitation (PLE) spectrum in Fig. 7a reveals that the absorptive $n\rightarrow\sigma^*$ (280 nm) and $\pi\rightarrow\pi^*$ (330 nm) transitions also lead to local maximum PL at 530 nm. Fig. 10 presents an explicit illustration of how the $\pi^*\rightarrow n$ transition is responsible for excitation-wavelength independent PL at 530 nm and relaxation of electrons from σ^* to π^* orbitals is essential for PL under short-wavelength excitation. The transition of electrons between the n state and π^* orbital for charge separation as well as recombination may involve phonon scattering to attain momentum alignment. The difference in energy between 470-nm excitation and 530-nm emission could be ascribed to phonon emissions involved in the electron transition between molecule orbitals. This energy difference would not result from the

presence of shallow trap states beneath the π* level because trap states between energy levels generally caused excitation-wavelength dependent emission.

3.4. GODs as a White-Emitting Phosphor

Fig. 11 presents one possible application of the GODs as a phosphor for white-light emission. As shown in Fig. 11a, the SLP-NGOD suspension is brown-yellow in color, while pure water is transparent to light. When illuminated with GaN-based violet light-emitting diodes (405 nm), the SLP-NGOD suspension exhibited strong white-light emissions (Fig. 11b), which resulted from a complementary combination of green PL and violet illumination. In contrast, the pure water did not respond to illumination at all. These results demonstrate the applicability of SLP-NGODs as a white-light emitting phosphor. Fig. 11c presents photographs of poly(vinyl alcohol) (PVA) polymer film embedded with SLP-NGODs and a bare PVA film. Tuning the content of the SLP-NGODs made it possible to obtain a PVA film that emits white light under violet-light irradiation (Fig. 11d).

4. Conclusions

This study demonstrated that GODs (2.5±0.5 nm) synthesized using mild and homogeneous oxidation of reduced GO sheets exhibit excitation-wavelength independent PL at 530 nm, which may correspond to the π*→n transition in the GODs in conjunction with an energy loss resulting from phonon scattering. The most effective excitation wavelength for PL occurred at an absorption wavelength of 470 nm, which provided energy for the n→π* transition and phonon absorption. Nitrogen

doping was shown to repair vacancy defects in the GODs and produce n-type conductivity, which compensated for the unbalanced charge in p-type GODs. This resulted in a suppression of charge leaks, which enhanced the PL *QY* from 16 % in uGODs to 22 % in NGODs. SLP treatment of uGODs and NGODs in THF resulted in the stabilization of oxygen functionalities through the transformation of C=O groups that served as active sites for charge leakage. The resulting SLP-uGODs and SLP-NGODs exhibited high PL *QY*s of 42 % and 50 %, respectively. When excited with violet light, the green light emitted from the GODs showed excellent performance in combining excitations to result in the emission of white light. This paper presents a strategy for material synthesis and the repair of vacancies and stabilization of functionalities to enable high-quality PL from GO-based species. The resulting materials show considerable promise for the synthesis of inexpensive, metal-free, environmentally-friendly phosphors for use in light-emitting devices.

Acknowledgements

This research was supported by the Ministry of Science and Technology, Taiwan (101-2221-E-006-243-MY3, 101-2221-E-006-225-MY3, 103-3113-E-006-009, and 102-3113-E-006-002), and by the Ministry of Education, Taiwan, The Aim for the Top University Project to the National Cheng Kung University.

† **Electronic Supplementary Information (ESI) available**: The XPS analysis results of uGODs; the PL emission results of uGODs and full-range PL spectra of NGODs; explanation of the Mott-Schottky equation; a summary of PL-spectra and the full-

range PL spectra of BGODs; the parameter values for PL quantum yield calculation.

See DOI: 10.1039/b000000x/.

References

1. S. N. Baker and G. A. Baker, *Angew. Chem. Int. Ed*., 2010, **49**, 6726-6744.
2. H. T. Li, Z. H. Kang, Y. Liu and S. T. Lee, *J. Mater. Chem*., 2012, **22**, 24230-24253.
3. S. J. Zhu, S. J. Tang, J. H. Zhang and B. Yang, *Chem. Commun*., 2012, **48**, 4527-4539.
4. J. H. Shen, Y. H. Zhu, X. L. Yang and C. Z. Li, *Chem. Commun*., 2012, **48**, 3686-3699.
5. Z. Liu, J. T. Robinson, X. M. Sun and H. J. Dai, *J. Am. Chem. Soc*., 2008, **130**, 10876-10877.
6. G. Eda , Y. Y. Lin , C. Mattevi , H. Yamaguchi , H. A. Chen , I. S. Chen , C. W. Chen and M. Chhowalla, *Adv. Mater*., 2010, **22**, 505-509.
7. D. Y. Pan, J. C. Zhang, Z. Li and M. H. Wu, *Adv. Mater*., 2010, **22**, 734-738.
8. J. Peng, W. Gao, B. K. Gupta, Z. Liu, R. R. Aburto, L. Ge, L. Song, L. B. Alemany, X. Zhan, G. Gao, S. A. Vithayathil, B. A. Kaipparettu, A. A. Marti, T. Hayashi, J. J. Zhu and P. M. Ajayan, *Nano Lett*., 2012, **12**, 844-849.
9. L. Cao, X. Wang, M. J. Meziani, F. Lu, H. Wang, P. G. Luo, Y. Lin, B. A. Harruff, L. M. Veca, D. Murray, S. Y. Xie and Y. P. Sun, *J. Am. Chem. Soc*., 2007, **129**, 11318-11319.
10. S. Chandra, P. Das, S. Bag, D. Laha and P. Pramanik, *Nanoscale*, 2011, **3**, 1533-1540.
11. S. K. Das, Y. Liu, S. Yeom, D. Y. Kim and C. I. Richards, *Nano Lett.*, 2014, **14**, 620-625.
12. T. F. Yeh, J. Cihlář, C.Y. Chang, C. Cheng and H. Teng, *Mater. Today*, 2013, **16**, 78-84.
13. K. P. Loh, Q. Bao, G. Eda and M. Chhowalla, *Nat. Chem*., 2010, **2**, 1015-1024.
14. Q. Mei, K. Zhang, G. Guan, B. Liu, S. Wang and Z. Zhang, *Chem. Commun*., 2010, **46**, 7319-7321.
15. K. J. Jeon, Z. Lee, E. Pollak, L. Moreschini, A. Bostwick, C. M. Park, R. Mendelsberg,

V. Radmilovic, R. Kostecki, T. J. Richardson and E. Rotenberg, *ACS Nano*, 2011, **5**, 1042-1046.

16. D. Pan, L. Guo, J. Zhang, C. Xi, Q. Xue, H. Huang, J. Li, Z. Zhang, W. Yu, Z. Chen, Z. Li and M. Wu, *J. Mater. Chem*., 2012, **22**, 3314-3318.
17. J. L. Chen, X. P. Yan, K. Meng and S. F. Wang, *Anal. Chem*., 2011, **83**, 8787-8793.
18. X. G. Peng, M. C. Schlamp, A. V. Kadavanich and A. P. Alivisatos, *J. Am. Chem. Soc*., 1997, **119**, 7019-7029.
19. Y. Shin, J. Lee, J. Yang, J. Park, K. Lee, S. Kim, Y. Park and H. Lee, *Small*, 2014, **10**, 866-870.
20. J. Shen, Y. Zhu, C. Chen, X. Yang and C. Li, *Chem. Commun*., 2011, **47**, 2580-2582.
21. F. Liu, M. H. Jang, H. D. Ha, J. H. Kim, Y. H. Cho and T. S. Seo, *Adv. Mater*., 2013, **25**, 3657-3663.
22. L Lin and S. Zhang, *Chem. Comm*., 2012, **48**, 10177-10179.
23. H. Sun, L. Wu, N. Gao, J. Ren and X. Qu, *ACS Appl. Mater. Interfaces*, 2013, **5**, 1174-1179.
24. J. Shen, Y. Zhu, X. Yang, J. Zong, J. Zhang and C. Li, *New J. Chem*., 2012, **36**, 97-101.
25. M. Li, W. Wu, W. Ren, H. M. Cheng, N. Tang, W. Zhong and Y. Du, *Appl. Phys. Lett*., 2012, **101**, 103107-3.
26. C. Hu, Y. Liu, Y. Yang, J. Cui, Z. Huang, Y. Wang, L. Yang, H. Wang, Y. Xiao and J. Rong, *J. Mater. Chem. B*, 2013, **1**, 39-42.
27. S. Dey, A. Govindaraj, K. Biswas and C. N. R. Rao, *Chem. Phys. Lett*., 2014, **595**, 203-208.
28. S. Zhu, J. Zhang, X. Liu, B. Li, X. Wang, S. Tang, Q. Meng, Y. Li, C. Shi, R. Hu and B. Yang, *RSC Adv*., 2012, **2**, 2717-2720.

29. D. B. Shinde and V. K. Pillai, *Chem. Eur. J.*, 2012, **18**, 12522-12528.

30. Y. Li, Y. Zhao, H. Cheng, Y. Hu, G. Shi, L. Dai and L. Qu, *J. Am. Chem. Soc.*, 2012, **134**, 15-18.

31. Z. Fan, Y. Li, X. Li, L. Fan, S. Zhou, D. Fang and S. Yang, *Carbon*, 2014, **70**, 149-156.

32. S. Zhuo, M Shao and S. T. Lee, *ACS Nano*, 2012, **6**, 1059-1064.

33. L. Tang, R. Ji, X. Cao, J. Lin, H. Jiang, X. Li, K. S. Teng, C. M. Luk, S. Zheng, J. Hao and S. P. Lau, *ACS Nano*, 2012, **6**, 5102-5110.

34. Y. Dong, J. Shao, C. Chen, H. Li, R. Wang, Y. Chi, X. Lin and G. Chen, *Carbon*, 2012, **50**, 4738-4743.

35. M. Hassan, E. Haque, K R. Reddy, A. I. Minett, J. Chen and V. G. Gomes, *Nanoscale*, 2014, **6**, 11988-11994.

36. L. H. Mao, W. Q. Tang, Z. Y. Deng, S. S. Liu, C. F. Wang and S. Chen, *Ind. Eng. Chem. Res.*, 2014, **53**, 6417-6425.

37. R. Sekiy, Y. Uemura, H. Murakami and T. Haino, *Angew. Chem. Int. Ed.*, 2014, **53**, 5725-5729.

38. C. T. Chien, S. S. Li, W. J. Lai, Y. C. Yeh, H. A. Chen, I. S. Chen, L. C. Chen, K. H. Chen, T. Nemoto, S. Isoda, M. W. Chen, T. Fujita, G. Eda, H. Yamaguchi, M. Chhowalla and C. W. Chen, *Angew. Chem. Int. Ed.*, 2012, **51**, 6662-6666.

39. K. Lingam, R. Podila, H. J. Qian, S. Serkiz and A. M. Rao, *Adv. Funct. Mater.*, 2013, **23**, 5062-5065.

40. Q. Su, S. P. Pang, V. Alijani, C. Li, X. L. Feng and K. Müllen, *Adv. Mater.*, 2009, **21**, 3191-3195.

41. Y. F. Xu, Z. B. Liu, X. L. Zhang, Y. Wang, J. G. Tian, Y. Huang, Y. F. Ma, X. Y. Zhang and Y. S. Chen, *Adv. Mater.*, 2009, **21**, 1275-1279.

42. M. de Miguel, M. Á lvaro and H. Garcí a, *Langmuir*, 2012, **28**, 2849-2857.

43. C. M. Hill, Y. Zhu and S. L. Pan, *ACS Nano*, 2011, **5**, 942-951.

44. T. Kuilla, S. Bhadra, D. H. Yao, N. H. Kim, S. Bose and J. H. Lee, *Prog. Polym. Sci*., 2010, **35**, 1350-1375.

45. Z. Zhang, H. H. Chen, C. Y. Xing, M. Y. Guo, F. G. Xu, X. D. Wang, H. J. Gruber, B. L. Zhang and J. L. Tang, *Nano Res*., 2011, **4**, 599-611.

46. I. V. Lightcap and P. V. Kamat, *J. Am. Chem. Soc*., 2012, **134**, 7109-7116.

47. G. Katsukis, J. Malig, C. Schulz-Drost, S. Leubner, N. Jux and D. M. Guldi, *ACS Nano*, 2012, **6**, 1915-1924.

48. L. Wang, S. J. Zhu, H. Y. Wang, Y. F. Wang, Y. W. Hao, J. H. Zhang, Q. D. Chen, Y. L. Zhang, W. Han, B. Yang and H. B. Sun, *Adv. Optical Mater*., 2013, **1**, 264-271.

49. H. Liu, Y. Liu and D. Zhu, *J. Mater. Chem*., 2011, **21**, 3335-3345.

50. T. Gokus, R. R. Nair, A. Bonetti, M. Böhmler, A. Lombardo, K. S. Novoselov, A. K. Geim, A. C. Ferrari and A. Hartschuh, *ACS Nano*, 2009, **3**, 3963-3968.

51. H. Wang, T. Maiyalagan and X. Wang, *ACS Catal*., 2012, **2**, 781-794.

52. T. F. Yeh, C. Y. Teng, S. J. Chen and H. Teng, *Adv. Mater*., 2014, **26**, 3297-3303.

53. M. Zhang, L. Bai, W. Shang, W. Xie, H. Ma, Y. Fu, D. Fang, H. Sun, L. Fan, M. Han, C. Liu and S. Yang, *J. Mater. Chem*., 2012, **22**, 7461-7467.

54. S. Liu, J. Tian, L. Wang, Y. Zhang, X. Qin, Y. Luo, A. M. Asiri, A. O. Al-Youbi and X. Sun, *Adv. Mater*., 2012, **24**, 2037-2041.

55. P. V. Kumar, M. Bernardi and J. C. Grossman, *ACS Nano*, 2013, **7**, 1638-1645.

56. X. Y. Li, H. Q. Wang, Y. Shimizu, A. Pyatenko, K. Kawaguchi and N. Koshizaki, *Chem. Commun*., 2011, **47**, 932-934.

57. L. Cao, P. Anilkumar, X. Wang, J. H. Liu, S. Sahu, M. J. Meziani, E. Myers and Y. P. Sun, *Can. J. Chem*., 2011, **89**, 104-109.

58. J. Senthilnathan, K. S. Rao and M. Yoshimura, *J. Mater. Chem. A*, 2014, **2**, 3332-3337.

59. J. Senthilnathan, Y. F. Liu, K. S. Rao and M. Yoshimura, *Sci. Rep*., 2014, **4**, 4395.

60. J. Senthilnathan, K. S. Rao, W. H. Lin, J. D. Liao and M. Yoshimura, *Carbon*, 2014, **78**, 446-454.

61. J. Senthilanthan, C. C. Weng, J. D. Liao and M. Yoshimura, *Sci. Rep*., 2013, **3**, 2414.

62. C. V. Pham, M. Krueger, M. Eck, S. Weber and E. Erdem, *Appl. Phys. Lett.* 2014, **104**, 132102.

63. S. Zhu, H. Zhang, P. Chen, L. H. Nie, C. H. Li and S. K. Li, *J. Mater. Chem. A*, 2015, **3**, 1540-1548.

64. K. P. Gong, F. Du, Z. H. Xia, M. Durstock and L. M. Dai, *Science*, 2009, **323**, 760-763.

65. C. Zhang, L. Fu, N. Liu, M. Liu, Y. Wang and Z. Liu, *Adv. Mater*., 2011, **23**, 1020-1024.

66. C. K. Chua and M. Pumera, *Chem. Soc. Rev*., 2014, **43**, 291-312.

67. T. Yoshimitsu, M. Tsunoda and H. Nagaoka, *Chem. Commun*., 1999, 1745-1764.

68. A. Eckmann, A. Felten, A. Mishchenko, L. Britnell, R. Krupke, K. S. Novoselov and C. Casiraghi, *Nano Lett*., 2012, **12**, 3925-3930.

69. B. D. Guo, Q. A. Liu, E. D. Chen, H. W. Zhu, L. A. Fang and J. R. Gong, *Nano Lett*., 2010, **10**, 4975-4980.

70. L. M. Malard, M. A. Pimenta, G. Dresselhaus and M. S. Dresselhaus, *Phys. Rep.*, 2009, **473**, 51-87.

71. D. Qu, M. Zheng, P. Du, Y. Zhou, L. G. Zhang, D. Li, H. Q. Tan, Z. Zhao, Z. G. Xie and Z. C. Sun, *Nanoscale*, 2013, **5**, 12272-12277.

72. P. C. Hsu, Z. Y. Shih, C. H. Lee and H. T. Chang, *Green Chem*., 2012, **14**, 917-920.

73. C. Fan, J. Xu, W. Chen, B. Lu, H. Miao, C. Liu and G. Liu, *J. Phys. Chem. C*, 2009, **113**, 9900-9910.

74. X. Wang, G. Sun, P. Routh, D.-H. Kim, W. Huang and P. Chen, *Chem. Soc. Rev.*, 2014, **43**, 7067-7098.

75. J. Shang, L. Ma, J. Li, W. Ai, T. Yu and G. G. Gurzadyan, *Sci. Rep*., 2012 , ***2***, 792.

76. B. E. Conway, Electrochemical Supercapacitors: Scientific Fundamentals and Technological Applications, Plenum Publishers, New York, USA, **1999**.

77. C. T. Hsieh and H. Teng, *Carbon* 2002, **40**, 667-674.

78. G. A. Crosby and J. N. Demas, *J. Phys. Chem*., 1971, **75**, 991-1023.

79. R. E. Kellogg and R. G. Bennett, *J. Chem. Phys*., 1964, **41**, 3042-3045.

80. A. öhrn and G. Karlström, *J. Phys. Chem. A*, 2006, **110**, 1934-1942.

81. M. Li, S. K. Cushing, X. Zhou, S. Guo and N. Wu, *J. Mater. Chem*., 2012, **10**, 23374-23379.

Table 1 (O 1s)/(C 1s) and (N 1s)/(C 1s) atomic ratio determined from the full-range XPS spectra and carbon bonding composition determined from the C 1s XPS (Fig. S1b, Fig. 3b, and Fig. 4) for uGODs, NGODs, and SLP-NGODs.

Sample	Atomic Ratio		Carbon Bonding Composition (%)				
	O1s/C1s	N1s/C1s	C-C	C-N	C-O	C=O	O-C=O
uGODs	0.53	--	66	--	8.0	22	3.9
NGODs	0.51	0.042	68	1.9	4.4	22	3.7
SLP-NGODs	0.52	0.036	67	1.6	16	8.4	7.2

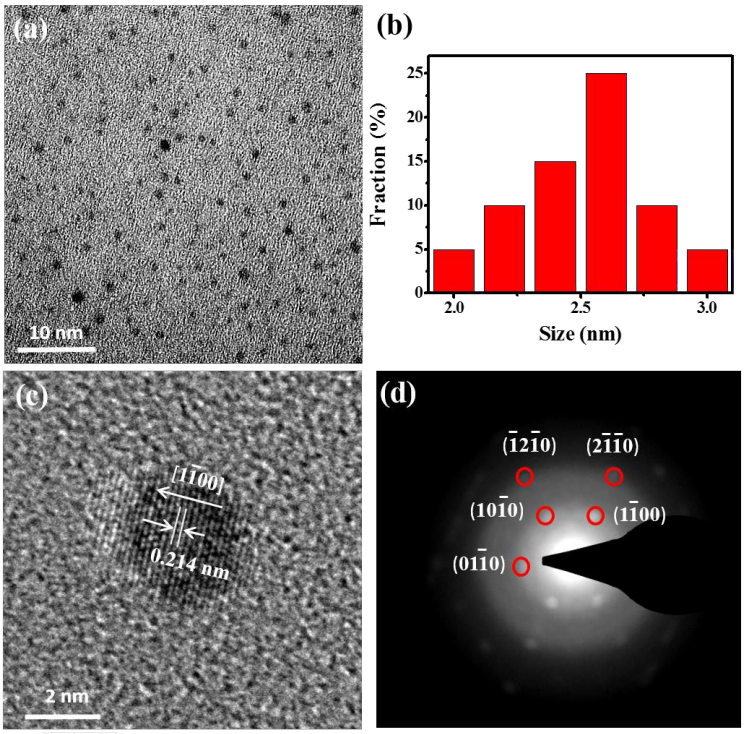

Fig. 1 Morphology and crystal structure of NGODs. (a) TEM image of NGODs. (b) Particle size distribution of NGODs. (c) High-resolution TEM image of NGODs, illustrating the graphene $\{1\bar{1}00\}$ lattice planes with a d-spacing of 0.214 nm. (d) The selected-area electron diffraction pattern of the NGODs in panel c.

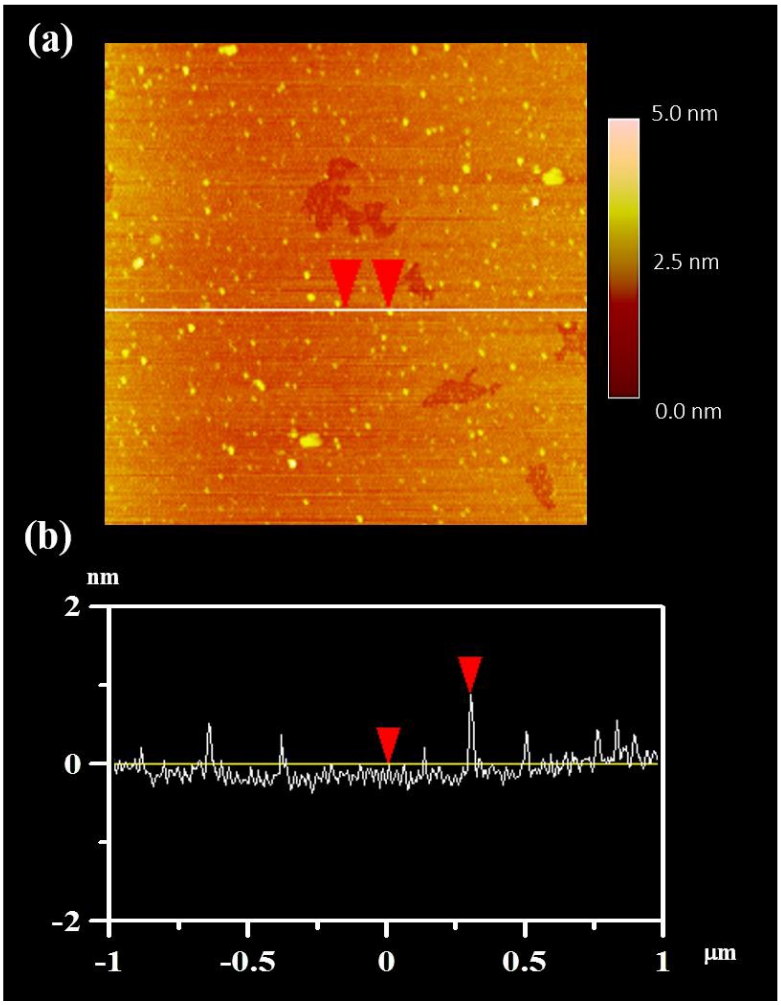

Fig. 2 Topographic analysis of NGODs. (a) AFM image of NGODs distributed on a mica substrate. (b) The height profile along the line of panel a.

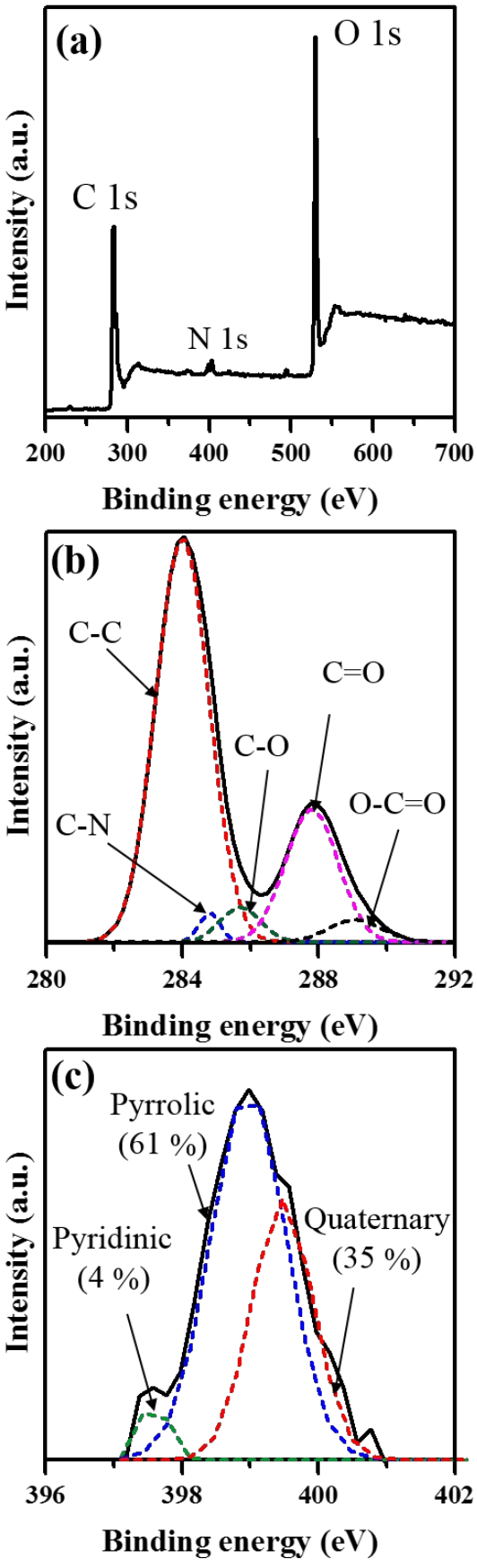

Fig. 3 XPS spectra of NGODs. (a) Full-range spectrum of NGODs. (b) C 1s spectrum of NGODs. (c) N 1s spectrum of NGODs. C 1s and N 1s spectra were decomposed into several peaks (indicated by the dash lines) that were fitted using a Gaussian function.

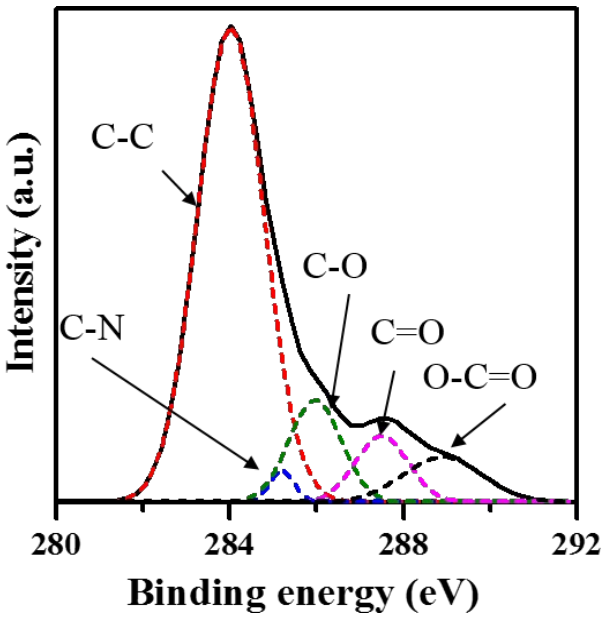

Fig. 4 C 1s XPS spectrum of the NGODs with SLP treatment in THF, i.e., SLP-NGODs. The spectrum was decomposed into several peaks (indicated by the dash lines) that were fitted using a Gaussian function.

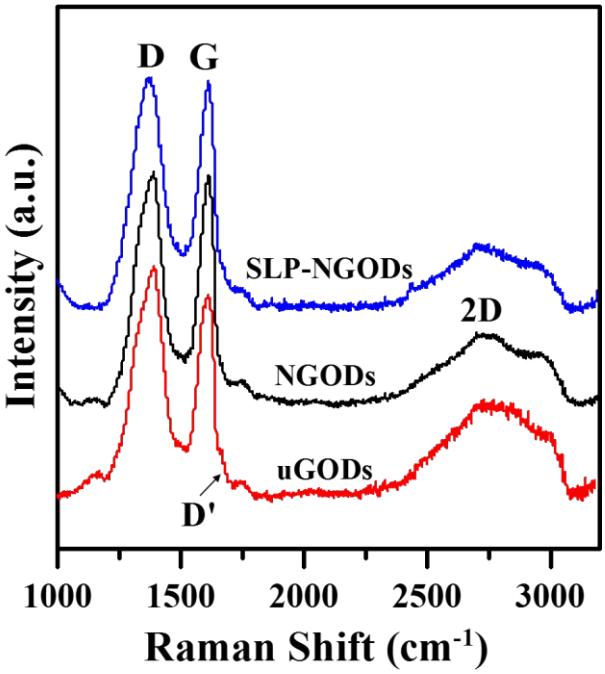

Fig. 5 Raman spectra of uGODs, NGODs, and SLP-NGODs.

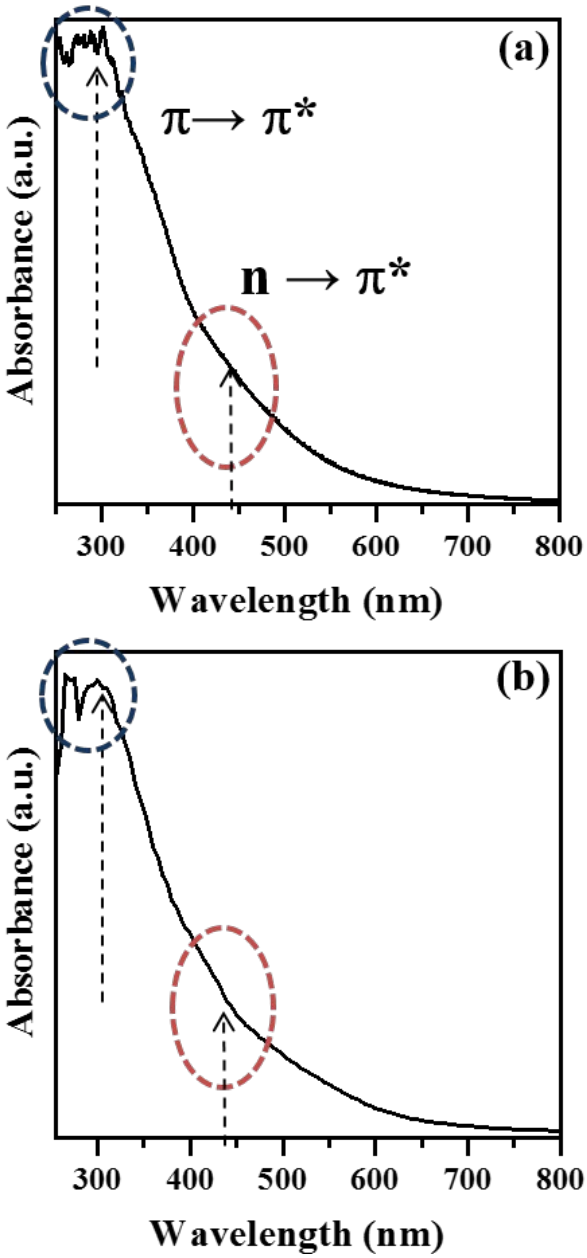

Fig. 6 Optical absorption spectra of the NGOD suspensions. (a) NGODs. (b) SLP-NGODs.

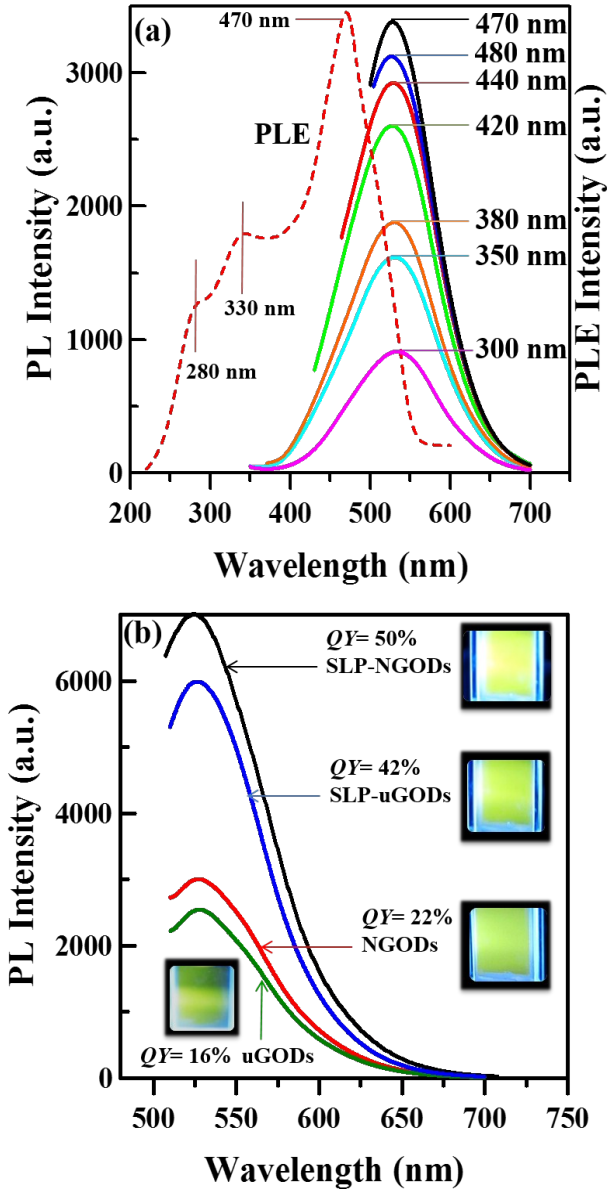

Fig. 7 PL spectra of the GODs. (a) NGODs excited by irradiation at various wavelengths. (b) uGODs, NGODs, SLP-uGODs, and SLP-NGODs excited by 470-nm irradiation. Panel a shows the PLE spectrum of NGODs for emissions at 530 nm (indicated by the dash line) and panel b contains insets that present photographs of the excited suspensions.

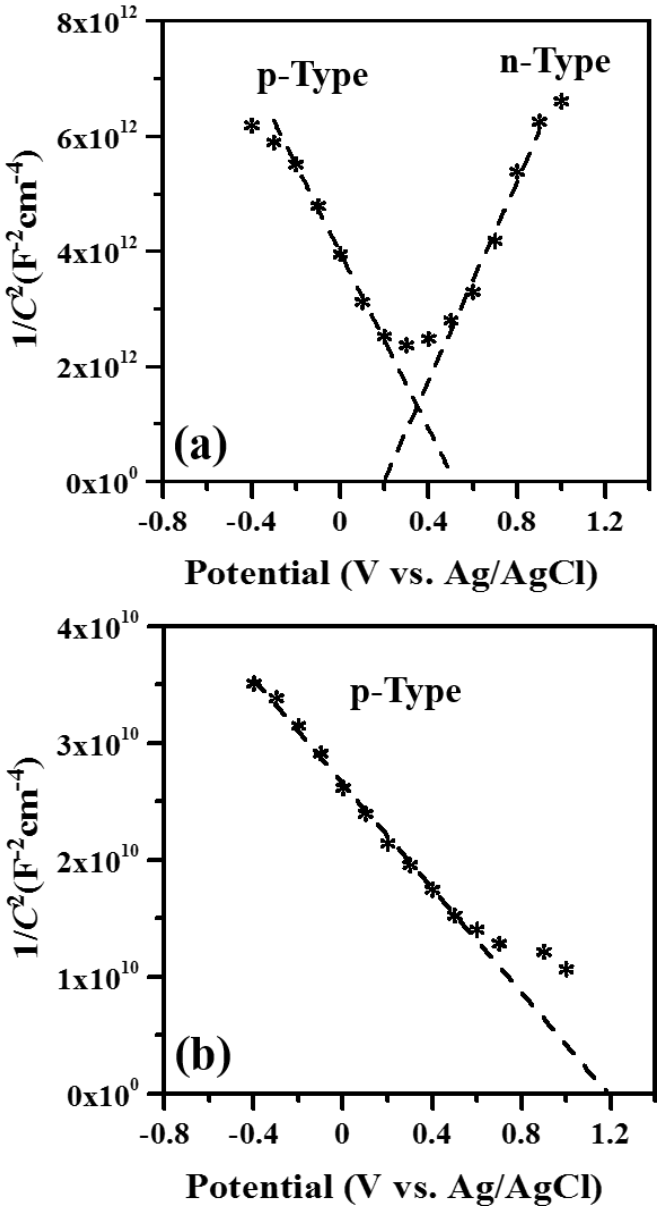

Fig. 8 Variation of capacitance (*C*) with the applied potential in 2 M H_2SO_4 presented in the Mott-shottky relationship for electrodes deposited with (a) NGODs and (b) uGODs. The capacitance was determined by electrochemical impedance spectroscopy. The negative and positive slopes correspond to p- and n-type conductivities, respectively.

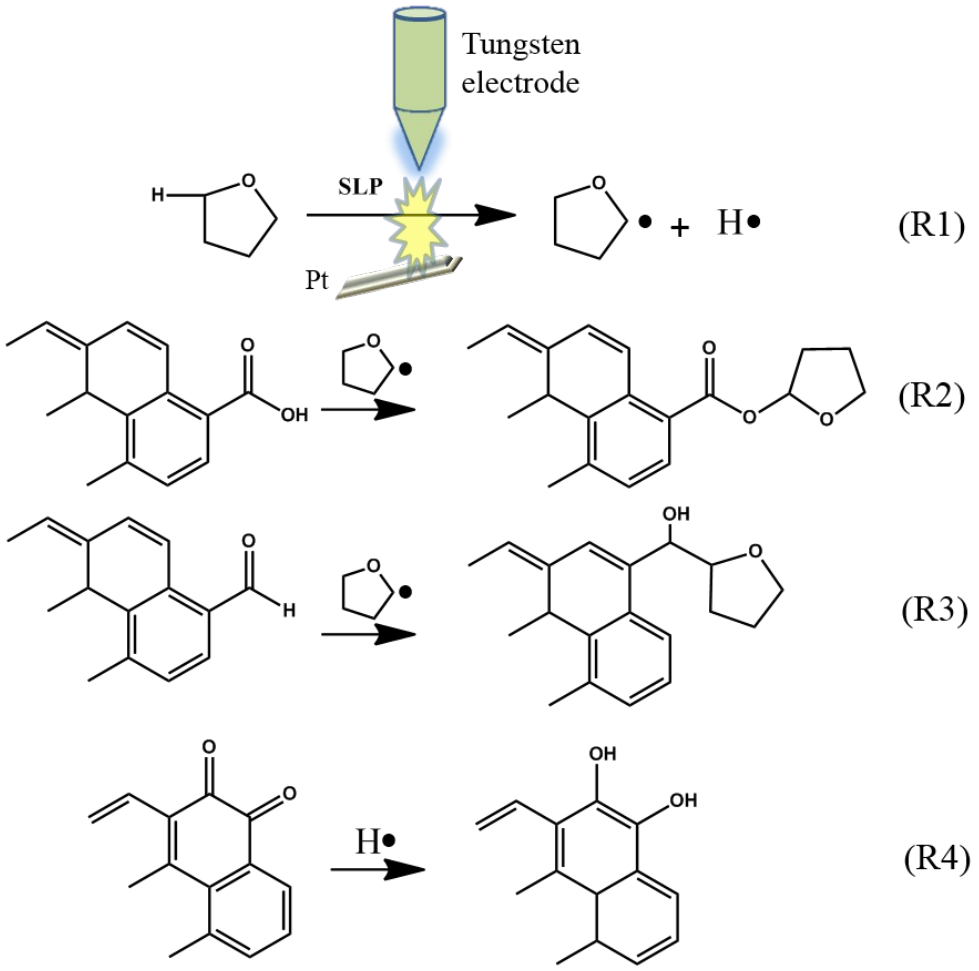

Fig. 9 A proposed mechanism for the transformation of aldehydes and ketones to stable ethers, alcohols, or esters through reactions R1–R4 with THF molecules. The inset in R1 presents a spark generated between a tungsten needle electrode and a platinum ground electrode in the SLP treatment.

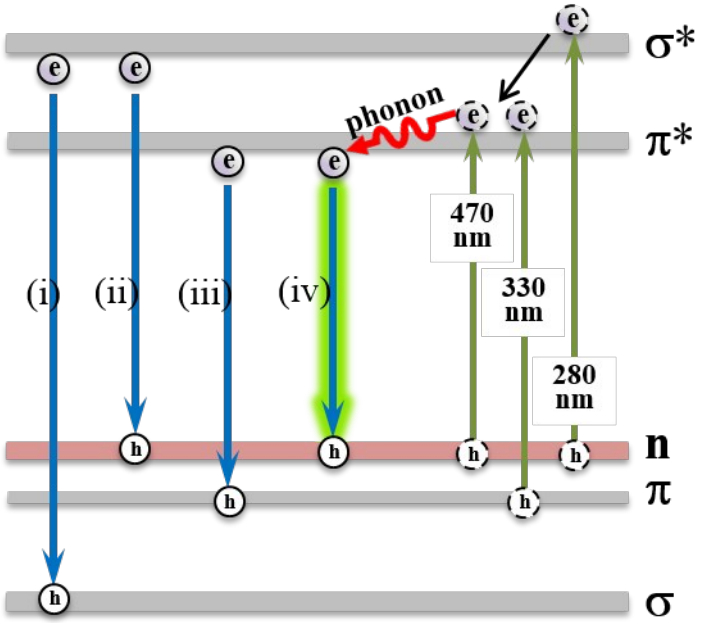

Fig. 10 A schematic diagram illustrating the energy levels associated with PL emissions from GO. (i) $\sigma^* \rightarrow \sigma$ recombination for alkane-like sp^3 domains. (ii) $\sigma^* \rightarrow n$ recombination that occurs in the sp^3 domains associated with hydroxyls, amines and ethers. (iii) $\pi^* \rightarrow \pi$ recombination that usually takes place in aromatic sp^2 domains. (iv) $\pi^* \rightarrow n$ recombination that is typically observed in sp^2 domains adjacent to ether, ketone, carboxyl, and ester groups. The $\pi^* \rightarrow n$ recombination is responsible for the excitation wavelength-independent PL at 530 nm and relaxation of electrons from σ^* to π^* orbitals is essential for PL under short-wavelength excitation.

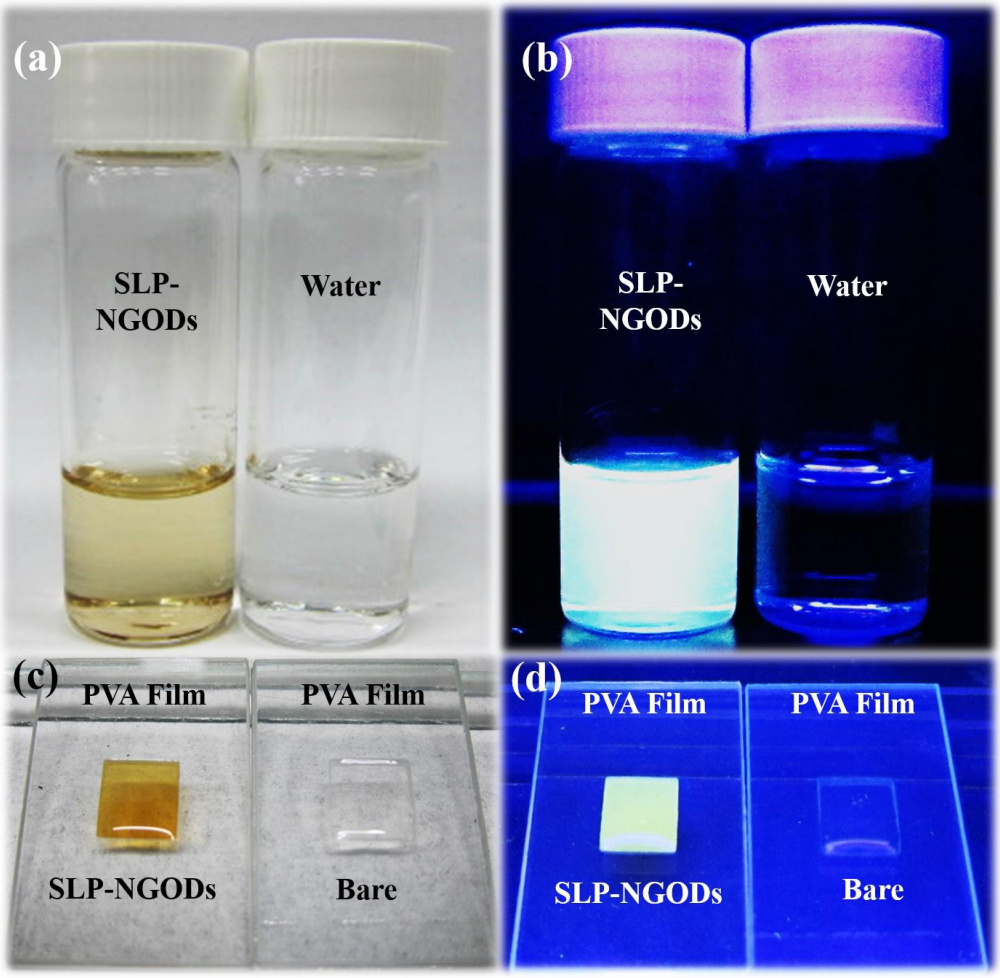

Fig. 11 Photographs of SLP-NGODs under different illuminations. (a) pure water and SLP-NGODs suspended in water under white-light illumination. (b) pure water and SLP-NGODs suspended in water under illumination with GaN-based violet light-emitting diodes (405 nm). (c) A bare PVA film and a PVA film embedded with SLP-NGODs under white-light illumination. (d) A bare PVA film and a PVA film embedded with SLP-NGODs under illumination with GaN-based violet light-emitting diodes (405 nm).

Table of Contents entry: Nitrogen-doped graphene oxide dots exhibit excitation-wavelength independent photoluminescence at 530 nm. Submerged liquid plasma treatment increases the photoluminescence quantum yield to 50 %. The dots show excellent white light emission by combining green emissions with violet light used for excitation.